Microscopic field-theoretical approach for mixtures of active and passive particles

Francesco Alaimo

Institute of Scientific Computing, Technische Universität Dresden, 01062 Dresden, Germany
and Dresden Center for Computational Materials Science (DCMS), 01062 Dresden, Germany

Axel Voigt[*]

Institute of Scientific Computing, Technische Universität Dresden, 01062 Dresden, Germany;
Dresden Center for Computational Materials Science (DCMS), 01062 Dresden, Germany;
and Center of Systems Biology Dresden (CSBD), Pfotenhauerstr. 108, 01307 Dresden, Germany

We consider a phase field crystal modeling approach for mixtures of interacting active and passive particles in two dimensions. The approach allows us to describe generic properties for such heterogeneous systems within a continuum model. We validate the approach by reproducing experimental results, as well as results obtained with agent-based simulations. The approach is valid for the whole spectrum from highly dilute suspensions of passive particles and interacting active particles in a dense background of passive particles. However, we concentrate only on the extreme cases, because for the situation with similar fractions of active and passive particles emerging structures are hard to analyze and experimental results are missing. We analyze in detail enhanced crystallization due to the presence of active particles, how collective migration is affected by a disordered environment, and laning states, which are globally nematic but polar within each lane.

I. INTRODUCTION

Active systems have been the focus of intense research for the last decade because they provide deep insights into the self-organization of systems that are intrinsically in a nonequilibrium state such as living matter. Even more interesting are mixtures of active and passive particles. Situations of active particles in crowded environments or passive particles in an active bath resemble the situation in living matter more realistically and might even shed light on the active dynamic processes within a cell [1]. Observed phenomena in mixtures of active and passive particles are, e.g., activity-induced phase separation [2], the formation of large defect-free crystalline domains [3], propagating interfaces [4], laning states [5] but also a transition from diffusive to subdiffusive dynamics [6,7], and suppressed collective motion [8]. To understand this wide span of phenomena is crucial to almost all applications of active systems.

Different ways exist to describe phenomena in active systems theoretically. Typical approaches for active systems consider either the microscopic scale, taking the interactions between the particles into account, or the macroscopic scale, focusing on the emerging phenomena. For reviews of both theoretical descriptions see, e.g., Refs. [9,10]. Examples for extensions towards mixtures of active and passive particles are summarized in Ref. [11] and range from active particles in confined domains [12–14], through active particles moving between fixed or moving obstacles [6,15–18], to binary mixtures of interacting active and passive particles

[2–5]. All these studies are examples for models on the microscopic scale. Most of these approaches consider the active particles as spherical particles which travel at a constant speed, whose direction changes according to interaction rules which comprise explicit alignment and noise. However, also without any explicit alignment rule, inelastic collisions [19] or deformations can lead to alignment [20]. Various more detailed microscopic models have been developed which model the deformation and internal processes within each particle [21,22]. These models are based on a phase field description of the particles and are computationally much more involved. In Refs. [23,24] another continuum modeling approach was introduced for active systems which combines aspects from the microscopic and the macroscopic scales. It can be viewed as a coarse-grained description of the phase field models [21,22]. Instead of describing the particles by a phase field function, particles are represented by peaks in a particle density field. Deformations and internal processes are still accounted for (see Ref. [24]), but the approach allows us to consider much larger numbers of particles, but still much lower than is possible with classical particle-based models.

The goal of the paper is to extend this coarse-grained continuum modeling approach to mixtures of active and passive particles, which will allow us to describe generic properties of such systems. We perform a preliminary study of binary collisions between active and passive particles, which provide useful predictions to understand how larger systems may evolve. We then use the model to study the effect of a few active particles in passive systems (active doping) [3,25,26], how passive particles perturb collective migration in an active bath [6,27–29], and in an intermediate regime the formation of lanes of active particles which move in opposite directions

———
[*]axel.voigt@tu-dresden.de

[5,20,30,31]. For the first case we observe enhanced crystallization in the passive system, in quantitative agreement with the results of Ref. [3]. For the active bath case we investigate how collective migration is affected by a disordered environment. For the special case of immobile passive particles these results are in agreement with Refs. [7,8]. However, for mobile passive particles new phenomena and patterns emerge, which ask for experimental validation. In the intermediate regime of similar fractions of active and passive particles a laning state is found, which is characterized by an alignment that is globally nematic but polar within each lane. This is in qualitative agreement with Ref. [5]. However, here it is also observed for spherical-like particles.

II. THE MODEL

The starting point for the derivation of the model is the microscopic field theoretical model for active particles introduced in Ref. [24]. It has been validated against known results obtained with minimal agent-based models and proven to be applicable for large-scale computations for thousands of particles. The model reads in scaled units

$$\partial_t \psi = M_0 \Delta \frac{\delta \mathcal{F}_{\text{vpfc}}}{\delta \psi} - v_0 \nabla \cdot (\psi \mathbf{P}),$$

$$\partial_t \mathbf{P} = \Delta(\alpha_2 \mathbf{P}) - (\alpha_4 \mathbf{P}) - v_0 \nabla \psi - \beta \mathbf{P} \mathbb{1}_{\psi_A \leqslant 0} \qquad (1)$$

for a one-particle density field $\psi(\mathbf{r}, t)$, which is defined with respect to a reference density $\bar{\psi}$.

We will interpret the peaks of ψ as particles. The polar order parameter $\mathbf{P}(\mathbf{r}, t)$, which is related to a coarse-grained velocity field with a typical magnitude v_0 of the self-propulsion velocity, models the internal processes within the particles. $\mathbf{P}$ is a local quantity that is different from zero only within the peaks of the density field ψ, which is ensured by $\beta > 0$ typically larger than the other terms entering the $\mathbf{P}$ equation and the Heaviside function $\mathbb{1}_{\psi_A \leqslant 0}$. $M_0 > 0$ is the mobility and $\alpha_2 > 0$ and $\alpha_4 > 0$ are two parameters related to relaxation and orientation of the polarization field. The influence of these parameters on the shape of the peaks, their inelastic collisions, and the resulting collective behavior is analyzed in detail in Ref. [24]. The energy functional $\mathcal{F}_{\text{vpfc}} = \mathcal{F}_{\text{pfc}} + \mathcal{F}_{\text{v}}$ consists of a Swift-Hohenberg energy [32]

$$\mathcal{F}_{\text{pfc}} = \int \left\{ \frac{1}{4} \psi^4 + \frac{1}{2} \psi [q + (1 + \Delta)^2] \psi \right\} d\mathbf{r}, \qquad (2)$$

with a parameter q related to temperature and a length scale 1 related to the lattice distance, and a penalization term

$$\mathcal{F}_{\text{v}} = \int H(|\psi|^3 - \psi^3) \, d\mathbf{r}, \qquad (3)$$

with $H \simeq 1500$ to constrain the one-particle density field ψ to positive values. The penalization term $\mathcal{F}_{\text{v}}$ is the essential modification which allows one to model individual particles [33–36]. Without this additional term the model can be related to models for active crystals [23,37] and be derived from dynamical density functional theory for Brownian systems [38,39]. See also the supplement in Refs. [23] and [40] for a detailed discussion and nondimensionalization of the equations.

If we, in addition, neglect the coupling with the polar order parameter $\mathbf{P}$ we obtain the classical phase field crystal (PFC) model introduced in Refs. [41,42] to model elasticity in crystalline materials. For a detailed derivation of (2) and its relation to classical density functional theory we refer to Refs. [43,44]. If the coupling with $\mathbf{P}$ is neglected but the penalization term (3) considered, the model is known as the vacancy PFC (VPFC) model [33].

Various ways have been introduced to extend the classical PFC model towards a second species, thus modeling binary mixtures [35,43]. We adopt one of these approaches for the VPFC model by considering energies for species A and B with

$$\mathcal{F}(\psi_A, \psi_B) = \mathcal{F}_{\text{vpfc}}^A(\psi_A) + \mathcal{F}_{\text{vpfc}}^B(\psi_B) + \mathcal{F}_{\text{int}}^{AB}(\psi_A, \psi_B), \qquad (4)$$

where $\mathcal{F}_{\text{vpfc}}^i$, $i = A, B$ as before and

$$\mathcal{F}_{\text{int}}^{AB}(\psi_A, \psi_B) = \frac{a}{2} \psi_A^2 \psi_B^2 \qquad (5)$$

is an interaction energy with $a > 0$.

In principle both species appearing in (4) could be made active. Our aim is, however, to simulate mixtures of interacting active and passive particles. With this in mind we couple only species A to the polar order parameter $\mathbf{P}$. For simplicity, we assume $\mathcal{F}_{\text{vpfc}}^A = \mathcal{F}_{\text{vpfc}}^B = \mathcal{F}_{\text{vpfc}}$ and thus, e.g., equal lattice distance of the active and passive particles. The resulting dynamical equations are

$$\frac{\partial \psi_A}{\partial t} = M_0^A \Delta \left[\frac{\delta \mathcal{F}(\psi_A)}{\delta \psi_A} + a \psi_A \psi_B^2 \right] - v_0 \nabla \cdot (\psi_A \mathbf{P}),$$

$$\partial_t \mathbf{P} = \alpha_2 \Delta \mathbf{P} - \alpha_4 \mathbf{P} - v_0 \nabla \psi_A - \beta \mathbf{P} \mathbb{1}_{\psi_A \leqslant 0},$$

$$\frac{\partial \psi_B}{\partial t} = M_0^B \Delta \left[\frac{\delta \mathcal{F}(\psi_B)}{\delta \psi_B} + a \psi_A^2 \psi_B \right], \qquad (6)$$

which define a microscopic field theoretical approach for binary mixtures of interacting active and passive particles. Extension to more than two species, species with different lattice distance and interaction potential, and active species with different self-propulsion velocities are obvious but will not be considered here.

III. RESULTS

We solve Eqs. (6) in two dimensions using a parallel finite element approach. We adopt a block-Jacobi preconditioner [45] that allows us to use a direct solver locally. This is implemented in AMDiS [46,47]. Details on the numerical approach can be found in Refs. [24,48]. The computational domain is a square of size $L = 200$ with periodic boundary conditions. The initial condition for ψ_A and ψ_B is calculated using a one-mode approximation with lattice distance $d = 4\pi/\sqrt{3}$ determined by the free energy equation (2) [36], with the centers placed randomly according to a packing algorithm [49]. The $\mathbf{P}$ field is set to zero initially.

Each maximum in the one-particle density fields ψ_A and ψ_B is interpreted as an active or passive particle, respectively. The diameter of the particle is defined by the lattice distance d. We track the particle positions $\mathbf{x}_{A,B}^i(t)$ and use this information to compute the particle velocities $\mathbf{v}_{A,B}^i(t)$ as the discrete time derivative of two successive maxima. We

TABLE I. Model parameters to be used in the simulations.

a	v_0	α_2	α_4	β	H	q
200	1.5	0.2	0.1	2	1500	−0.9

define the total particle density $\phi = N\sigma/L^2$, with N the total number of particles $N = N_A + N_B$ and $N_{A,B}$ the number of A and B particles, respectively. The parameter $\sigma = \pi(d/2)^2$ is the area occupied by a single particle. The fraction of active particles present in the system is $\eta_A = N_A/N$. When a small fraction of particles is active ($\eta_A < 0.2$) we are in the regime of active doping and analyze how a passive system is influenced by the presence of a few active particles. Increasing the number of active particles ($\eta_A > 0.7$) we are in the regime of an active bath and study how a few passive particles affect an active system.

Unless otherwise specified in the figure captions, we fix the parameters shown in Table I.

A. Binary collisions between active and passive particles

We begin with analyzing a binary collision of an active and a passive particle. Figures 1(a) and 1(b) show the results for two different values of the mobility of the passive particle, $M_0^B = 10$ (left) and $M_0^B = 70$ (right). At time $t = 0$ a passive particle [shown as a black (transparent gray) disk] is placed at the origin. An active particle, shown as a fixed contour line of ψ_A, is placed a few lattice lengths to the left with a homogeneous polarization directed towards the right. For the low-mobility case ($M_0^B = 10$, left) the active particle bounces back after colliding with the passive particle, which does not move. This is confirmed by a plot of the x component of the velocity for both particles [Fig. 1(c)].

For the opposite case of high mobility ($M_0^B = 70$, right) the passive particle is transported along the x axis by the active particle [the black arrow in Fig. 1(b) represents the trajectory of the passive particle]. The x components of the velocities

shown in Fig. 1(d)) confirm this. The collision causes a slowing of the active particle and results in a movement of the active and the passive particle with the same velocity.

This preliminary analysis shows that for low values of the passive mobility M_0^B passive particles can act as fixed obstacles. In this case a collision causes a change in the active particle direction. However, for large values of M_0^B the passive particle is transported by the active particle. The active particle does not change its direction, only the velocity decreases. These qualitative differences will also affect larger systems, which will be analyzed next.

B. Active doping: How active particles enhance crystallization

It has been shown by particle simulations [25,26] and experimentally [3] that the crystalline structure of passive particles is altered by the presence of active agents. More precisely active particles generate density variations in the passive system and promote crystallization, leading to the formation of passive clusters. To analyze these phenomena with our microscopic field theoretical approach we need to identify if a particle belongs to a cluster. We follow the definition of Ref. [3] where two criteria have to be fulfilled. The nearest neighbor distances are less than $3/2d$, and the coordination number is six.

Figure 2 shows snapshots with passive clusters for different η_A and ϕ. The time evolution of the percentage of passive particles which belong to a cluster X_f is shown in Fig. 3. For dilute systems [$\phi = 0.5$, Fig. 2(a)] X_f slowly increases with time. Increasing the fraction of active particles η_A leads to larger values X_f. However, it remains relatively low, rarely exceeding 20%, for the considered time ($t = 1000$). Increasing the density [$\phi = 0.6$, Fig. 2(b)] the system changes from a state where no clusters are present ($t = 0$) to a state where up to 50% of the passive particles are found in clusters. A maximum X_f is observed for $\eta_A = 0.1$, where X_f saturates at $t = 1000$. Further increasing the number of active particles leads to a reduction of X_f. Adding more and more active
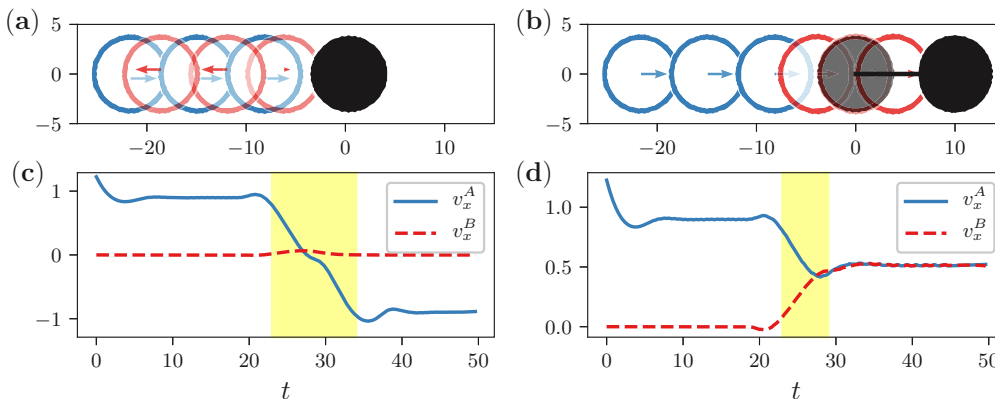
FIG. 1. (a), (b) Time series of a head-on collision between an active and a passive particle for low passive mobility $M_0^B = 10$ (a) and high passive mobility $M_0^B = 70$ (b). The active particle is shown (at different times) as a contour line of ψ_A, and its orientation is represented by an arrow. Blue (red) is used to show the particle before (after) the collision. The final position of the passive particle is shown as a black disk, whereas in (b) the transparent black disk represents the initial condition of the passive particle, and the black line its trajectory. The active particle bounces back after the collision (a) and transport the passive particle (b). The velocities along the x direction of active and passive particles are shown as a function of time in panels (c) for $M_0^B = 10$ and (d) for $M_0^B = 70$; $M_0^A = 70$ for both cases. The yellow region represents the approximate time of the collision.
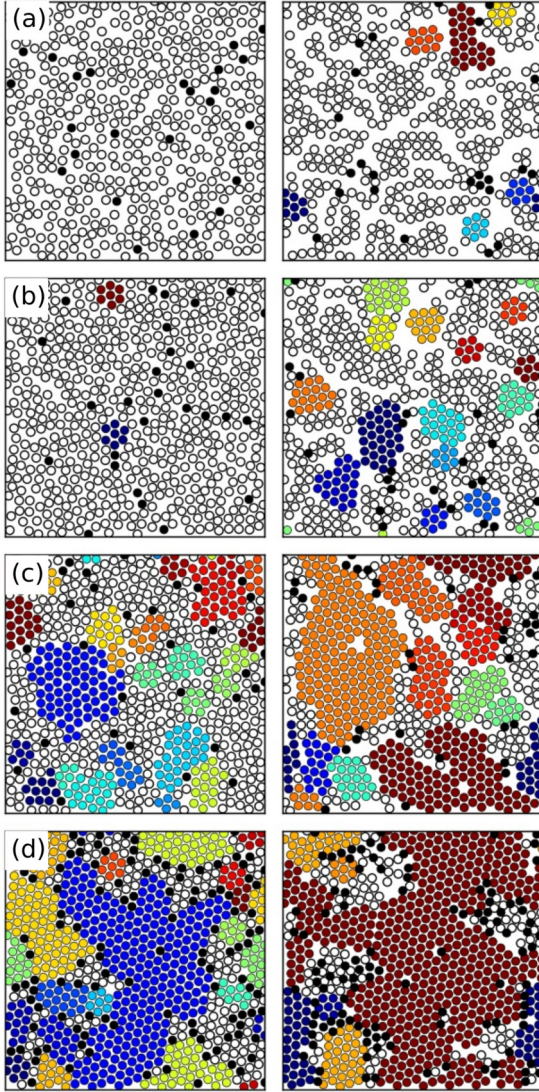
FIG. 2. Snapshots showing passive clusters for different total densities and fractions of active particles ϕ and η_A at time $t = 0$ (first column) and at time $t = 1000$ (second column). Particles with the same color belong to the same cluster, white disks represent passive particles not belonging to any cluster, and black disks are active particles. (a) $\phi = 0.5$, $\eta_A = 0.05$, (b) $\phi = 0.6$, $\eta_A = 0.05$ (c) $\phi = 0.7$, $\eta_A = 0.05$, (d) $\phi = 0.8$, $\eta_A = 0.15$. Other parameters are $M_0^A = M_0^B = 50$.

particles to systems with already existing crystalline clusters introduces disorder, a phenomenon already observed in Ref. [3]. By further increasing the density [$\phi = 0.7$, Fig. 2(c)] some clusters are already present for the random initial configuration at $t = 0$, due to spontaneous crystallization. Active particles can be inside these regions, thus disturbing their symmetry. This explains why the system behaves in the opposite way as for the dilute case, with X_f decreasing as the fraction of active particles η_A increases. Finally for $\phi = 0.8$ the initial configuration is already almost completely crystallized [$X_f \simeq 1$ for $t = 0$, Fig. 2(d)]. Adding active particles partially destroys the crystalline structure (Fig. 3) and X_f decreases for increasing η_A. We thus observe both

phenomena: enhanced crystallization in dilute systems and suppressed crystallization in dense systems.

A final observation concerns how the dynamics of the active particles is affected by the presence of passive ones. In Fig. 4 the maximum of the particle-averaged mean square displacement $\langle \Delta r^2(t) \rangle$ for active particles is shown as a function of ϕ and η_A. No data are shown for $\eta_A = 0.01$, as the number of active particles is too small for meaningful averages. We observe a clear correlation between this value and the crystallization in the system: the higher X_f, the smaller the maximum displacement of active particles until, for the extreme case of $\phi = 0.8$ and $\eta_A = 0.05$, active particles are trapped inside a big passive cluster and show a very small displacement (see also Supplemental video SV1 in Ref. [50]).

C. Active bath: How passive particles can suppress collective migration

Inelastic collisions in systems which are composed solely of active particles can lead to collective motion. This has been shown by particle-based models (e.g., Ref. [19]), microscopic field theoretical models [24], and phase field models [21,22]. In all these models the state of collective migration is characterized by the order parameter $\omega = 1/N_A | \sum_{i=1}^{N_A} \hat{\mathbf{v}}_A^i(t) |$ being close to one, with $\hat{\mathbf{v}}_A^i(t)$ the unit velocity vector for the active particle i at time t. We analyze here the stability of the state of collective motion, if passive particles are introduced in the system. How do the total density, the fraction of active particles, and the mobility of passive particles affect this state?

To consider a dense system, we fix $\phi = 0.9$ and further set $\eta_A = 0.9$. We have seen (Fig. 1) that for low mobility M_0^B passive particles act as fixed objects. The situation is therefore comparable with experimental studies for active colloids in disordered environments [8], which show a suppression of collective motion. Also in our simulations the active system does not reach a state of collective motion, as shown from the time series of ω [Fig. 5(b)]. However, the situation changes if we increase M_0^B, thus making the passive particles mobile. Figure 5(a) shows the average velocity $\tilde{\mathbf{v}}_B$ of the passive particles as a function of their mobility. Increasing M_0^B, the average passive particles' velocity $\tilde{\mathbf{v}}_B$ also increases, meaning that passive particles are transported by the active ones, as expected. The order parameter ω does not always increase monotonically with M_0^B. In Fig. 5(b) we see, for instance, that ω has a slightly higher value for $M_0^B = 10$ (red curve) than for $M_0^B = 30$ (blue curve). This is true also for higher values of M_0^B, but we can say that for $M_0^B = 50, 70$ a state of collective migration is reached [Fig. 5(b)], even though the time required to reach it is larger than in the homogeneous case $\eta_A = 1$ (no passive particles present).

We now fix the mobility $M_0^B = 70$ and vary ϕ and η_A. We reduce ϕ down to 0.7, a limit for which a state of collective migration would still be reached in a homogeneous active system ($\eta_A = 1$), as seen from the purple lines in Fig. 6. For $\phi = 0.9$ a state of collective migration is reached for $\eta_A = 0.9$ but with a longer transient phase than for the homogeneous case [green line in Fig. 6(c)]. For $\eta_A = 0.8$ we already see a small perturbation from the unit value for ω, and for $\eta_A = 0.7$ collective migration is no longer reached. We observe here the accumulation of passive particles in certain regions; see also
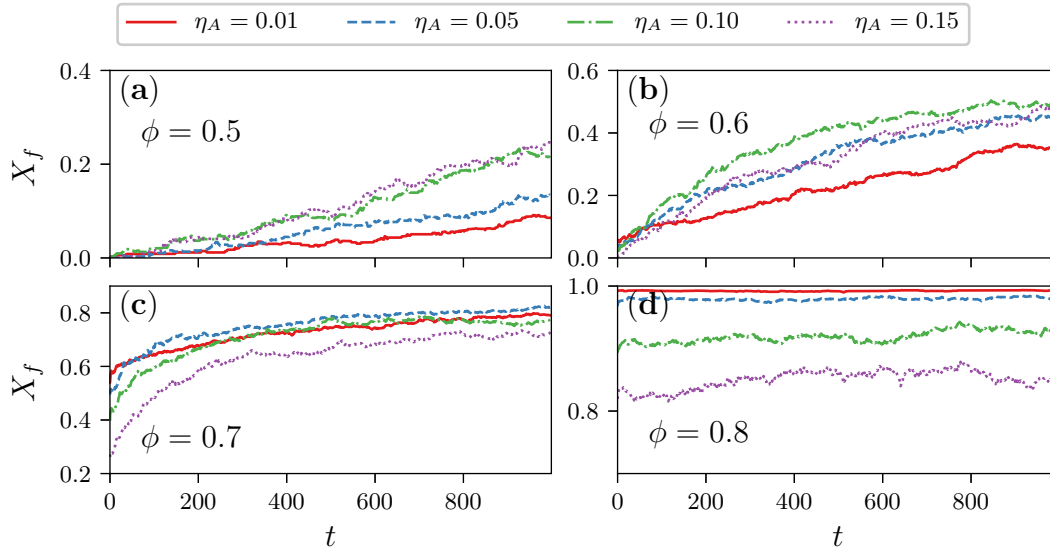
FIG. 3. Percentage of passive particles belonging to a cluster X_f as a function of time for different total densities and fractions of active particles ϕ and η_A. We observe that for $\phi = 0.5$ and $\phi = 0.6$ (top row), increasing the number of active particles leads to an increase of X_f, whereas the opposite is true for $\phi = 0.7$ and $\phi = 0.8$ (bottom row). Other parameters are $M_0^A = M_0^B = 50$. Each curve has been obtained as the average of five different simulations starting with different initial conditions.

Fig. 7(d). This hinders the active particles from following a straight trajectory and thus the formation of collective migration. Things change by reducing the total density to $\phi = 0.8$. The state of collective migration is not reached, independently of the value of η_A [Fig. 6(b)]. However, for $\eta_A = 0.9$, the green curve in Fig. 6(b), a new state is formed, where the order parameter ω is at least locally close to one. This new state is discussed below and can be seen in the snapshots in Figs. 7(a) and 7(b). For $\phi = 0.7$ [Fig. 6(a)] a decrease in η_A leads to a decrease of ω. In this situation there is enough empty space in the system to allow active particles to change their trajectories when interacting with passive ones. This causes a perturbation that gets bigger as the number of passive particles increases, leading to a decrease of ω.

A more detailed investigation of the intermediate regime with $\phi = 0.8$ and $\eta_A = 0.9$ [Figs. 7(a) and 7(b)] shows an intermediate state with two lanes of active particles moving in opposite direction. The lanes are separated by passive particles (black disks) that prevent the alignment of the collectively migrating domains. It is more stable in Fig. 7(a), persisting for the whole simulation time, and less stable in Fig. 7(b), where the alignment of passive particles will be destroyed after a while and a transition to collective migration follows (see Supplemental video SV2 in Ref. [50]). This state is known as a laning state, and it is characterized by an alignment that is globally nematic but polar within each lane. It has already been observed for self-propelled rods with an effective nematic alignment [30,31], soft deformable self-propelled particles with high aspect ratio [20], and a mixture
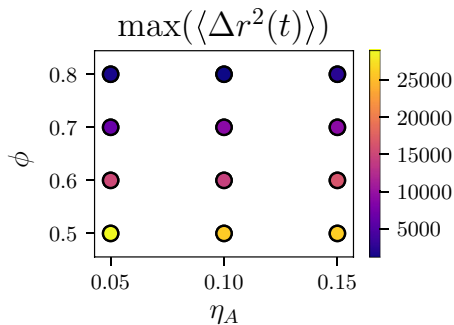
FIG. 4. Maximum of the particle-averaged mean square displacement $\langle \Delta r^2(t) \rangle$ of active particles moving in a binary mixture for different values of ϕ and η_A. Active particles travel a longer distance when the passive particles have not crystallized, until the extreme case of $\phi = 0.8$, $\eta_A = 0.05$ where the maximum mean square displacement is so low that active particles are basically trapped (see also Supplemental video SV1 in Ref. [50]). Other parameters are $M_0^A = M_0^B = 50$. Each point has been obtained as the average of five different simulations started with different initial conditions.
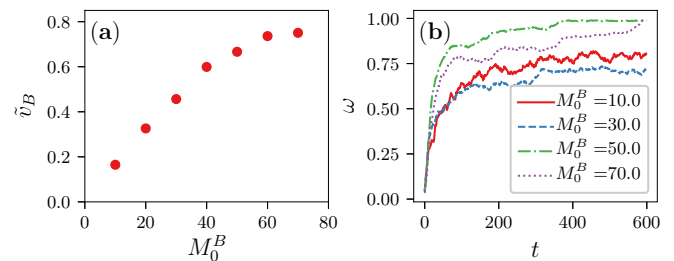
FIG. 5. (a) Average velocity $\tilde{v}_B$ of passive particles as a function of their mobility in an active bath with $\phi = 0.9$, $\eta_A = 0.9$. $\tilde{v}_B$ increases almost linearly for small M_0^B until it starts to saturate at around $M_0^B = 70$. (b) Order parameter ω as a function of time for different mobility M_0^B. For small values of M_0^B there is no collective migration, for intermediate values this state is reached quite fast, whereas for high mobility the transient phase to reach collective migration increases. We choose to fix $M_0^B = 70$ for the analysis in Fig. 6. $M_0^A = 100$ for both cases. The data have been obtained as the average of 10 different simulations started with different initial conditions.
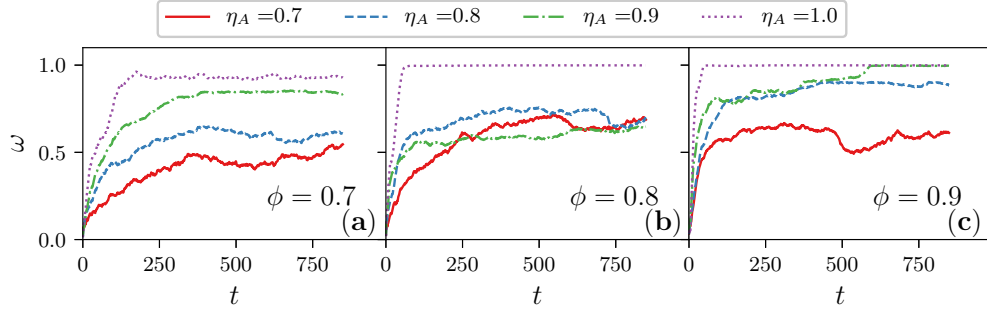
FIG. 6. Order parameter ω as a function of time for different values of ϕ and η_A. The purple curve corresponds to the case $\eta_A = 1$, i.e., no passive particles present. We see that in all other cases the state of collective migration is reached later (longer transient phase) or not reached at all, especially for lower η_A (red curves). Other parameters are $M_0^A = 100$ and $M_0^B = 70$. The data have been obtained as the average of 10 different simulations begun with different initial conditions.

of self-propelled and passive rods interacting solely through excluded volume interactions [5]. It is to our knowledge the first time that this laning state is observed in a mixture of interacting spherical-like particles whose velocity alignment would be globally polar in the absence of passive particles [24].

Even if a state of pure collective migration is reached, the passive particles are not randomly distributed but are transported by the active particles, filling the holes between them. For $\phi \simeq 0.8$ the packing of the collectively migrating active particles allows the passive particles to arrange in the free space. They form chainlike structures [Fig. 7(c) and

FIG. 7. The color code corresponds to the orientation of the single-particle velocity, and black disks represent passive particles. (a) Snapshot of a laning state, with two macroregions of active particles having exactly opposite orientation. This state can last for a long time because of the presence of passive particles at the boundary between the two regions (see also Supplemental video SV2 in Ref. [50]). (b) Another laning state. Here less passive particles are accumulated at the boundary between the moving active regions. This situation is less stable, and, at a later time (c), active particles all move in the same direction, whereas passive ones form chains, which persist over longer periods (see also Supplemental video SV3 in Ref. [50]). (d) Passive particles forming clusters in an active bath. (a)–(c) Regime $\phi = 0.8$, $\eta_A = 0.9$, (d) regime $\phi = 0.9$, $\eta_A = 0.7$.

Supplemental video SV3 in Ref. [50]], which persist over longer periods and are transported by the active particles. If the number of passive particles is increased $\eta_A = 0.7$ a clustering of passive particles within the active bath can be observed; see Fig. 7(d). These new states and patterns are characteristic for binary mixtures and should be explored further, both numerically and experimentally.

IV. CONCLUSIONS

In summary, our microscopic field theoretical approach for mixtures of interacting active and passive particles has been used to investigate a wide spectrum from systems with $\phi < 0.7$ to dense systems $\phi > 0.7$ with a relatively low fraction of active particles $\eta_A < 0.2$ (active doping) and a relatively high fraction $\eta_A > 0.7$ (active bath), respectively. We have demonstrated with one and the same model a variety of known phenomena, such as enhanced crystallization via active doping [3,25] and suppressed crystallization in dense systems [3]. We also analyzed the limits of collective migration, which for the special case of immobile passive particles qualitatively reproduce the results in Ref. [8]. Within the experiments in Ref. [3] and in our simulations the suppression of collective migration sensitively depends on the fraction of immobile passive particles. Within the experimentally less explored state of mobile passive particles we found distinct phenomena. For fractions of passive particles, for which collective migration is suppressed if the passive particles are immobile, collective motion is still possible if the mobility of these particles is large enough. But there are also intermediate regimes, known as laning states, where lanes of active particles moving in opposite direction are separated by boundary layers of passive ones. We further found chains of passive particles and clusters which persist for a relatively long time. A rigorous classification of these states remains open and should be addressed with experimental investigations.

While the approach is unable to reach system sizes possible with classical particle-based methods, it provides a minimal approach for a more detailed microscopic description, which does not need any explicit alignment rule, accounts for processes within the particle, and allows for particle deformations. It can be seen as a coarse-grained description of the phase field models [21,22]. As already pointed out, the approach can easily be modified to consider more than two

species, species with different size and interaction potential, and active species with different self-propulsion velocities, which makes the approach a generic tool to study active systems in complex environments. Also hydrodynamic interactions have already been considered together with a (passive) phase field crystal model [36,51] and could also be included in the considered model.

[1] A. Das, A. Polley, and M. Rao, Phys. Rev. Lett. **116**, 068306 (2016).

[2] J. Stenhammar, R. Wittkowski, D. Marenduzzo, and M. E. Cates, Phys. Rev. Lett. **114**, 018301 (2015).

[3] F. Kümmel, P. Shabestari, C. Lozano, G. Volpe, and C. Bechinger, Soft Matter **11**, 6187 (2015).

[4] A. Wysocki, R. G. Winkler, and G. Gompper, New J. Phys. **18**, 123030 (2016).

[5] S. R. McCandlish, A. Baskaran, and M. F. Hagan, Soft Matter **8**, 2527 (2012).

[6] M. Zeitz, K. Wolff, and H. Stark, Eur. Phys. J. E **40**, 23 (2017).

[7] A. Morin, D. Lopes Cardozo, V. Chikkadi, and D. Bartolo, Phys. Rev. E **96**, 042611 (2017).

[8] A. Morin, N. Desreumaux, J.-B. Caussin, and D. Bartolo, Nat. Phys. **13**, 63 (2017).

[9] M. C. Marchetti, J. F. Joanny, S. Ramaswamy, T. B. Liverpool, J. Prost, M. Rao, and R. A. Simha, Rev. Mod. Phys. **85**, 1143 (2013).

[10] S. Ramaswamy, Annu. Rev. Condens. Matter Phys. **1**, 323 (2010).

[11] C. Bechinger, R. Di Leonardo, H. Löwen, C. Reichhardt, G. Volpe, and G. Volpe, Rev. Mod. Phys. **88**, 045006 (2016).

[12] G. Briand, M. Schindler, and O. Dauchot, Phys. Rev. Lett. **120**, 208001 (2018).

[13] E. Lushi and C. S. Peskin, Comput. Struct. **122**, 239 (2013).

[14] H. Wioland, F. G. Woodhouse, J. Dunkel, J. O. Kessler, and R. E. Goldstein, Phys. Rev. Lett. **110**, 268102 (2013).

[15] C. J. O. Reichhardt and C. Reichhardt, New J. Phys. **20**, 025002 (2018).

[16] C. Reichhardt and C. J. O. Reichhardt, J. Phys.: Condens. Matter **30**, 015404 (2018).

[17] A. Kaiser, H. H. Wensink, and H. Löwen, Phys. Rev. Lett. **108**, 268307 (2012).

[18] A. Kaiser, K. Popowa, H. H. Wensink, and H. Löwen, Phys. Rev. E **88**, 022311 (2013).

[19] D. Grossman, I. S. Aranson, and E. Ben Jacob, New J. Phys. **10**, 023036 (2008).

[20] A. M. Menzel and T. Ohta, EPL (Europhy. Lett.) **99**, 58001 (2012).

[21] J. Löber, F. Ziebert, and I. S. Aranson, Sci. Rep. **5**, 9172 (2015).

[22] W. Marth and A. Voigt, Interface Focus **6**, 20160037 (2016).

[23] A. M. Menzel and H. Löwen, Phys. Rev. Lett. **110**, 055702 (2013).

[24] F. Alaimo, S. Praetorius, and A. Voigt, New J. Phys. **18**, 083008 (2016).

[25] R. Ni, M. A. Cohen Stuart, M. Dijkstra, and P. G. Bolhuis, Soft Matter **10**, 6609 (2014).

[26] B. van der Meer, M. Dijkstra, and L. Filion, Soft Matter **12**, 5630 (2016).

[27] X. L. Wu and A. Libchaber, Phys. Rev. Lett. **84**, 3017 (2000).

[28] C. Valeriani, M. Li, J. Novosel, J. Arlt, and D. Marenduzzo, Soft Matter **7**, 5228 (2011).

[29] D. F. Hinz, A. Panchenko, T.-Y. Kim, and E. Fried, Soft Matter **10**, 9082 (2014).

[30] H. Wensink, J. Dunkel, S. Heidenreich, K. Drescher, R. Goldstein, H. Lowen, and J. Yeomans, Proc. Natl. Acad. Sci. USA **109**, 14308 (2012).

[31] H. Wensink and H. Löwen, J. Phys.: Condens. Matter **24**, 464130 (2012).

[32] J. Swift and P. C. Hohenberg, Phys. Rev. A **15**, 319 (1977).

[33] P. Y. Chan, N. Goldenfeld, and J. Dantzig, Phys. Rev. E **79**, 035701 (2009).

[34] J. Berry and M. Grant, Phys. Rev. Lett. **106**, 175702 (2011).

[35] M. J. Robbins, A. J. Archer, U. Thiele, and E. Knobloch, Phys. Rev. E **85**, 061408 (2012).

[36] S. Praetorius and A. Voigt, J. Chem. Phys. **142**, 154904 (2015).

[37] A. M. Menzel, T. Ohta, and H. Löwen, Phys. Rev. E **89**, 022301 (2014).

[38] U. M. B. Marconi and P. Tarazona, J. Chem. Phys. **110**, 8032 (1999).

[39] A. J. Archer and R. Evans, J. Chem. Phys. **121**, 4246 (2004).

[40] H. H. Wensink and H. Löwen, Phys. Rev. E **78**, 031409 (2008).

[41] K. R. Elder, M. Katakowski, M. Haataja, and M. Grant, Phys. Rev. Lett. **88**, 245701 (2002).

[42] K. R. Elder and M. Grant, Phys. Rev. E **70**, 051605 (2004).

[43] K. R. Elder, N. Provatas, J. Berry, P. Stefanovic, and M. Grant, Phys. Rev. B **75**, 064107 (2007).

[44] S. van Teeffelen, R. Backofen, A. Voigt, and H. Löwen, Phys. Rev. E **79**, 051404 (2009).

[45] S. Praetorius and A. Voigt, SIAM J. Sci. Comput. **37**, B425 (2015).

[46] S. Vey and A. Voigt, Comput. Visual. Sci. **10**, 57 (2007).

[47] T. Witkowski, S. Ling, S. Praetorius, and A. Voigt, Adv. Comput. Math. **41**, 1145 (2015).

[48] R. Backofen, A. Rätz, and A. Voigt, Phil. Mag. Lett. **87**, 813 (2007).

[49] M. Skoge, A. Donev, F. H. Stillinger, and S. Torquato, Phys. Rev. E **74**, 041127 (2006).

[50] See Supplemental Material at http://link.aps.org/supplemental/10.1103/PhysRevE.98.032605 for Supplemental movies.

[51] V. Heinonen, C. V. Achim, J. M. Kosterlitz, S.-C. Ying, J. Lowengrub, and T. Ala-Nissila, Phys. Rev. Lett. **116**, 024303 (2016).